Structural Engineering and Mechanics, Vol. 30, No. 2 (2008) 191-209 191
DOI: http://dx.doi.org/10.12989/sem.2008.30.2.191

System identification of a building structure using wireless MEMS and PZT sensors

Hongjin Kim†, Whajung Kim‡ and Boung-Yong Kim‡†

School of Architecture & Civil Engineering, Kyungpook National University, Korea

Jae-Seung Hwang‡‡

School of Architecture, Chonnam National University, Gwangju, Korea

(Received August 31, 2007, Accepted May 2, 2008)

Abstract. A structural monitoring system based on cheap and wireless monitoring system is investigated in this paper. Due to low-cost and low power consumption, micro-electro-mechanical system (MEMS) is suitable for wireless monitoring and the use of MEMS and wireless communication can reduce system cost and simplify the installation for structural health monitoring. For system identification using wireless MEMS, a finite element (FE) model updating method through correlation with the initial analytical model of the structure to the measured one is used. The system identification using wireless MEMS is evaluated experimentally using a three storey frame model. Identification results are compared to ones using data measured from traditional accelerometers and results indicate that the system identification using wireless MEMS estimates system parameters with reasonable accuracy. Another smart sensor considered in this paper for structural health monitoring is Lead Zirconate Titanate (PZT) which is a type of piezoelectric material. PZT patches have been applied for the health monitoring of structures owing to their simultaneous sensing/actuating capability. In this paper, the system identification for building structures by using PZT patches functioning as sensor only is presented. The FE model updating method is applied with the experimental data obtained using PZT patches, and the results are compared to ones obtained using wireless MEMS system. Results indicate that sensing by PZT patches yields reliable system identification results even though limited information is available.

Keywords: MEMS; PZT; health monitoring; system identification; FE model updating.

1. Introduction

Structural health monitoring has been gaining more and more importance in civil engineering areas such earthquake and wind engineering (Lee and Yun 2006, Gao and Spencer 2007). The use of health monitoring system can also provide tools for the validation of structural analytical model. However, only few structures such as historical buildings and some important long bridges have been

† Assistant Professor, E-mail: hjk@knu.ac.kr
‡ Professor, Corresponding author, E-mail: kimwj@knu.ac.kr
‡† Graduate Student, E-mail: dragon1053@knu.ac.kr
‡‡ Assistant Professor, E-mail: jshwang@jnu.ac.kr

instrumented with structural monitoring system due to high cost of installation and long and complicated installation of system wires (Lynch *et al*. 2003).

In this paper, a structural monitoring system based on cheap and wireless monitoring system is investigated. Recently, micro-electro-mechanical system (MEMS) became one of the most rapidly developing technologies for the structural health monitoring (Obadat *et al*. 2003, Staszewski *et al.* 2004, Zhang *et al*. 2005). MEMS is a small integrated device or system that combines electrical and mechanical components. It ranges in size from the sub micrometer level to the millimeter level. For MEMS, the term *micro* suggests a literally small system, *electro* suggests electricity and/or electronics, and mechanical suggests moving parts of some kind (Lin and Wang 2006). Examples of MEMS devices range over sensors for airbag systems, miniature robots, microengines, inertial sensors, and chemical, pressure and flow sensors. These systems can be utilized for sensing, control, or actuator technology in micro-scale (Vittorio 2001, Hierold 2004).

The basic operation of a MEMS accelerometer is as a spring-mass system, where a set of springs suspends a mass on the chip. As the device accelerates, the inertia of the mass causes the springs to stretch and compress until the spring-force equals the applied force and the mass accelerates with the device. Deflection of the spring is measured using a differential capacitor that consists of independent fixed plates and plates attached to the moving mass. As the mass moves, it changes the distance between the plates of a parallel plate capacitor, which induces a differential capacitance in the system. Sensitive signal conditional circuitry then amplifies and filters the signal, producing an analog voltage proportional to the acceleration (Helvajian 1999).

The MEMS accelerometer has advantages of small size, low-cost, and low power consumption, and thereby is suitable for wireless monitoring (Shinozuka *et al.* 2003). Consequently, the use of advanced technology of MEMS and wireless communication can reduce system cost and simplify the installation for the structural health monitoring. Further, the application of wireless MEMS system can provide enhanced system functionality due to low noise densities (Kinawi *et al*. 2002, Krüger *et al*. 2005).

For system identification using wireless MEMS, a finite element (FE) model updating method is used in which the system parameters are updated by correlating initial analytical model of a structure to the measured one. The FE model updating method minimizes the variation of system matrices such as stiffness and mass matrices based on modal properties while satisfying the appropriate constraints (Baruch and Bar-Itzhack 1978). Since the FE model updating is performed using measured natural frequencies and mode shapes, it has an advantage that the system identification is possible with limited information (Friswell and Mottershead 1995). The system identification using wireless MEMS is evaluated experimentally using a three storey frame model. Identification results are compared to ones using data measured from traditional accelerometers and results indicate that the system identification using wireless MEMS estimates system parameters quite accurately.

Another smart sensor considered in this paper for structural health monitoring is based on piezoelectric materials, such as PZT, often referred to as piezoceramic patches or PZT patches. PZT material is being applied for the health monitoring of structures due to its simultaneous sensing/actuating capability. Recently, extensive research on the damage detection using PZT materials has been performed based on experimental data (Park *et al*. 2003, Tseng Wang 2004). These researchers mostly utilized the impedance manipulation using input voltage and output current. These methods, however, often require somewhat high magnitude of input voltage to vibrate a structure globally, thus a significantly large, sometimes practically impossible, input voltage is needed to measure the impedance of a large structure especially at low frequencies. Consequently, the system identification based on sensing/actuating PZT materials is not easy for large structures such as high rise buildings. Recently, research on electro-mechanical impedance (EMI) techniques has been performed to overcome this problem. In the EMI technique, a PZT patch operates in 30-300 kHz range with small voltages of the order of 1 Volt and hence excites the local modes of a structure (Soh *et al*. 2000, Bhalla and Soh 2004). In this paper, the system identification for building structures by using PZT functioning as sensor only is presented. The FE model updating method is applied with the experimental data obtained using PZT patches, and the results are compared to ones obtained using wireless MEMS system.

2. Wireless MEMS system

The wireless MEMS system consists of three parts: 1) MEMS accelerometer, 2) wireless transmitter, and 3) wireless receiver. The interface between the receiver and PC or notebook computer is through common LAN port using TCP/IP communication. Up to seven wireless transmitters can be connected to one receiver, and multiple receivers can be connected to PC using a network HUB system, which is a device for connecting multiple fiber optic Ethernet devices together.

2.1 MEMS accelerometer

MEMS sensor evaluated for this research is the ADXL103 from Analog Devices. The ADXL103 is precision, low power, complete single axis accelerometer. It has a measuring range of ±1.7 g, and can measure both static and dynamic accelerations. The output is analog voltage proportional to acceleration with a nominal scale factor of 1 V/g. The dimension of MEMS sensor is 5 mm × 5 mm × 2 mm. The more detailed accelerometer properties are summarized in Table 1.

Table 1 ADXL103 accelerometer specification

Parameter	Typical values
SENSOR INPUT	
Measurement Range	± 1.7 *g*
Nonlinearity	± 0.2%
SENSITIVITY	
Sensitivity (Vs = 5V)	1000 mV/*g*
Sensitivity change due to Temperature	±0.3%
Resolution	1 mg at 60 Hz
ZERO g BIAS LEVEL	
0 *g* Voltage	2.5 V
Initial 0 *g* Output deviation from ideal	±25 m*g*
0 *g* offset vs. temperature	±0.1 mg/°C
NOISE PERFORMANCE	
Output noise	1 mV rms
Noise density	110 μg/√Hz rms
FREQUENCY RESPONSE	
Sensor resonant frequency	5.5 kHz

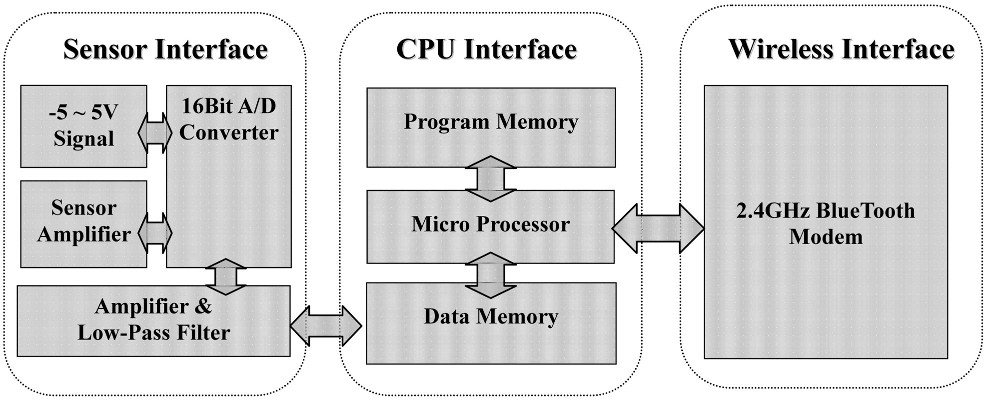

Fig. 1 Schematic layout of wireless transmitter

2.2 Wireless transmitter

The wireless transmitter performs three functions as illustrated in Fig. 1. In the sensor interface, input analog signals from sensor units are amplified, low-pass filtered, and transformed into digital signals using analog-to-digital (A/D) converter. The amplification factors of 1 to 3000 and low-pass filters of 10 to 1000 Hz are available and can be controlled remotely. The A/D conversion resolution is 16-bits and sampling rate of up to 1000 Hz can be attained. In this study, the basic antenna with communication distance of 120 m is used. The communication range can be increased up to 1000 m with special antenna.

Digitized data is saved into internal flash memory so that all data can be recovered in case of communication malfunctioning or battery discharge, and is transmitted to the wireless receiver through universal asynchronous receiver/transmitter (UART) port, which is an integrated circuit used for serial communications over a computer or peripheral device, and BlueTooth Modem. Other than BlueTooth such as IEEE 802.11 and radio frequency (RF) modulated wireless communications with bandwidth of 900 MHz or 433 MHz can be attained due to common UART port. In order to

(a) Wireless transmitter (b) Wireless transmitter (inside) (c) Wireless receiver

Fig. 2 Fully assembled wireless transmitter and receiver units minimize the power consumption, hardware and software are designed to support sleep/wake up function. In Fig. 2, the wireless transmitter unit is presented along with wireless receiver unit.

3. System Identification of a building using MEMS accelerometers

Experiments for the system identification using wireless MEMS system are performed in Chonnam National University, Korea. The schematic of the shaking table experiment of a three storey building equipped with wireless MEMS system is presented in Fig. 3, and Fig. 4 shows photographs of the building and sensors. The storey height of the building is 40 cm and measured storey mass is 22.5 kg. Four MEMS accelerometers are installed to measure floor acceleration including base floor, and additional four piezoelectric accelerometers are installed to verify the MEMS data. The piezoelectric accelerometers used in the experiment are LC0116A from Lance Measurement Technologies Co., Ltd. Both MEMS sensors and piezoelectric accelerometers are connected to wireless transmitter units using a small wire for the wireless monitoring. The mass of each set of MEMS sensor and wireless transmitter is 0.258 kg.

3.1 System identification and FE model updating

When the mass matrix of the structure is obtainable from FE modeling, the stiffness matrix can be updated based on the measured data with following two constraints: 1) the updated stiffness matrix reproduces measured modal data, and 2) is symmetric as follows (Baruch 1978).

$$\mathbf{K}_{up}\mathbf{\Phi}_{up} = \mathbf{M}_{a}\mathbf{\Phi}_{up}\mathbf{\Lambda} \tag{1}$$

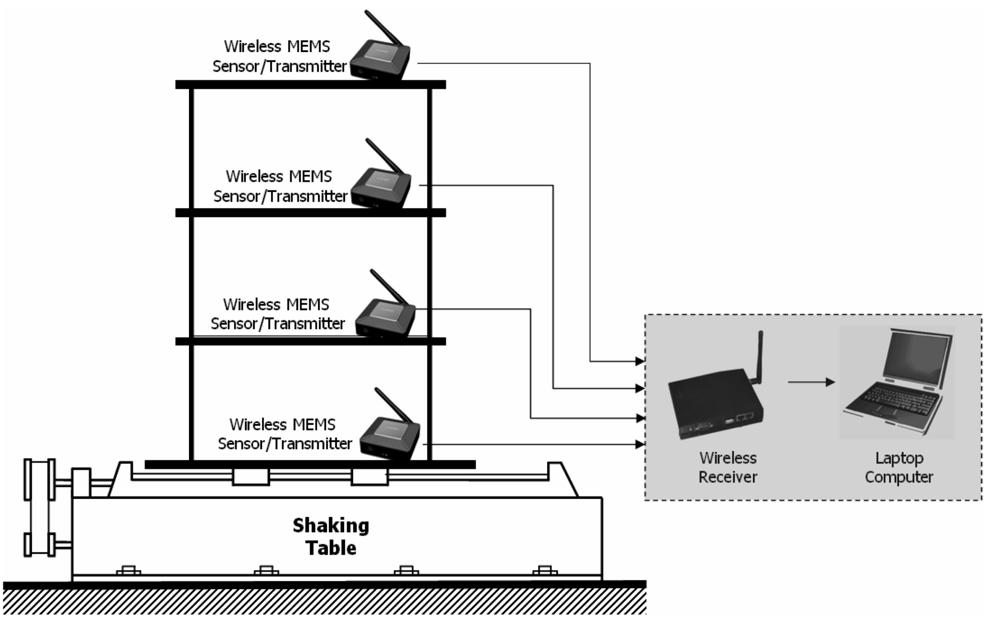

Fig. 3 Schematic of the shaking table experiment of a three storey building with wireless MEMS

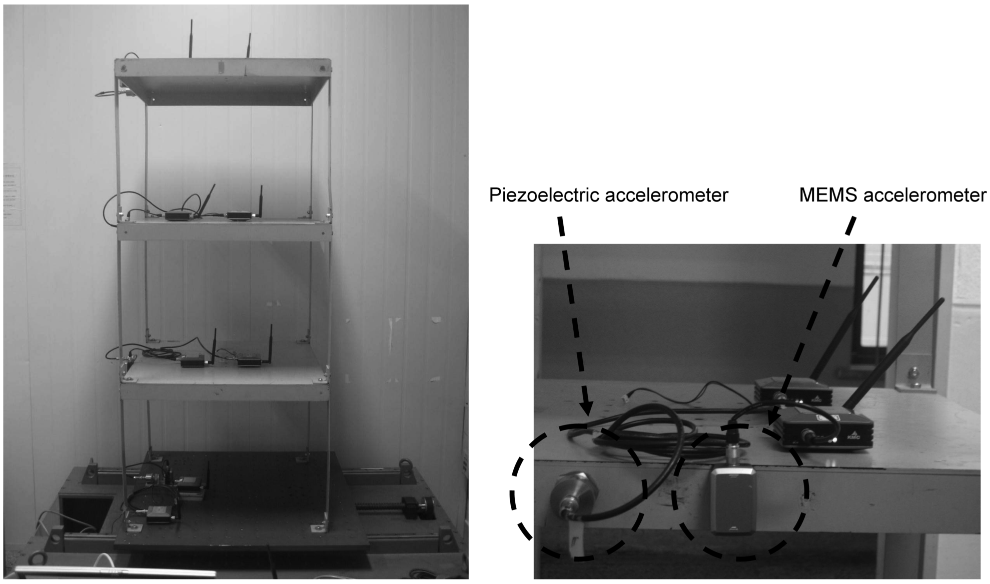

(a) Three storey building (b) MEMS and traditional accelerometers

Fig. 4 Experimental setup for the system identification using wireless MEMS system

$$\mathbf{K}_{up}^{T} = \mathbf{K}_{up} \tag{2}$$

where $\boldsymbol{M}_a$ is the analytically obtained mass matrix, $\boldsymbol{K}_{up}$ is the stiffness matrix to be updated, is a diagonal matrix with the measured natural frequencies squared on the diagonal, and $\boldsymbol{\Phi}_{up}$ is the eigenvectors to be updated using measured eigenvectors as

$$\mathbf{\Phi}_{up} = \mathbf{\Phi}_m[\mathbf{\Phi}_m^T\mathbf{M}_a\mathbf{\Phi}_m]^{-1/2} \tag{3}$$

where $\boldsymbol{\Phi}_m$ is the measured eigenvectors. The stiffness matrix, which satisfies constraints in Eqs. (1) and (2), is updated by minimizing the difference between the updated stiffness matrix and analytically derived stiffness matrix as defined in Eq. (4).

$$J = \frac{1}{2}\left\|\mathbf{N}^{-1}(\mathbf{K}_{up}-\mathbf{K}_a)\mathbf{N}^{-1}\right\| \tag{4}$$

where $\mathbf{N} = \mathbf{M}_a^{1/2}$ and $\boldsymbol{K}_a$ is the analytically obtained stiffness matrix. The resulting updated stiffness matrix is

$$\mathbf{K}_{up} = \mathbf{K}_a - \mathbf{K}_a\mathbf{\Phi}_{up}\mathbf{\Phi}_{up}^T\mathbf{M}_a - \mathbf{M}_a\mathbf{\Phi}_{up}\mathbf{\Phi}_{up}^T\mathbf{K}_a + \mathbf{M}_a\mathbf{\Phi}_{up}\mathbf{\Phi}_{up}^T\mathbf{K}_a\mathbf{\Phi}_{up}\mathbf{\Phi}_{up}^T\mathbf{M}_a + \mathbf{M}_a\mathbf{\Phi}_{up}\mathbf{\Lambda}\mathbf{\Phi}_{up}^T\mathbf{M}_a \tag{5}$$

The frequency response function (FRF) and mode shape vectors are obtained from the measured data using Eqs. (6) and (7). If the adjacent modal frequencies are distinct and thereby each modal resonance response is not affected by other modes, then the resonant FRF for absolute acceleration of i-th floor from ground acceleration is (Li and Reinhorn 1995).

$$T_{ai}(\omega_k) = \phi_{ik}H_{ik}(\omega_k)\Gamma_k \tag{6}$$

where $T_{ai}(\omega_k)$ and $H_{ik}(\omega_k)$ are the resonant and non-resonant FRFs of k-th mode for absolute acceleration of i-th floor from ground acceleration, respectively, ϕ_{ik} is the (i, k)th element of $\mathbf{\Phi}_m$, and Γ_k is the k-th scalar of $\Gamma = -\mathbf{\Phi}_m^T \mathbf{M}_a \mathbf{E}$ where $\mathbf{E}$ is the ground acceleration influence matrix. For k-th mode, the ratio of i-th component to j-th component of the modal vector can be estimated calculating the ratio of absolute acceleration FRFs.

$$\phi_{ik}/\phi_{jk} = T_{ai}(\omega_k)/T_{aj}(\omega_k) \tag{7}$$

3.2 Free vibration test

A free vibration test is performed to validate the wireless MEMS accelerometers. The first five second of acceleration response time history of the third floor is presented in Fig. 5. As shown in Fig. 5, MEMS accelerometers exhibit less noise level compared to the piezoelectric accelerometers.

Fig. 6 shows the free vibration responses of three floors, and Fig. 7 shows their frequency responses from MEMS accelerometers. It can be noticed from Fig. 7 that the first mode vibration governs the free vibration. The second mode is detected slightly, and the third mode is not visible. The first and second natural frequencies obtained from the free vibration test are 0.90 Hz and 2.67 Hz. The estimated first mode eigenvector using Eq. (7) is $\boldsymbol{\phi}_1^T = [0.5180 \;\; 0.8453 \;\; 1.0]$. Modal damping ratio for the first mode only is estimated since the second mode is not vibrated enough. As the first mode governs, the first modal damping ratio is estimated using the logarithmic decrement method. The third floor acceleration is used for the estimation, and the estimated damping ratio is 0.50%. Fig. 8 shows the third floor response time history and the estimated envelope function. As shown in Fig. 8, the estimated envelope function closely represents the vibration decaying.

When the mass matrix is given, there exist infinite numbers of stiffness matrices that give the estimated first modal frequency. The test building structure, however, is fabricated such that each floor has identical columns. Therefore, the storey stiffness can be obtained using the first modal

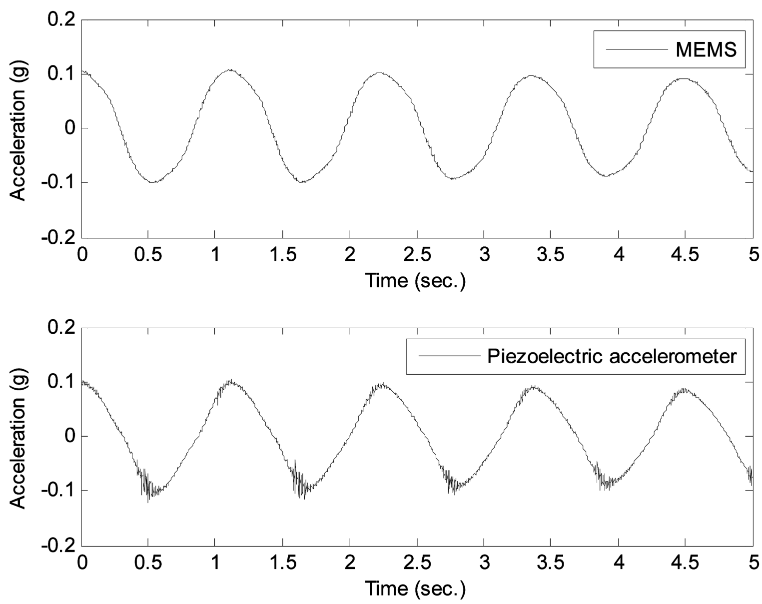

Fig. 5 Acceleration response time history of the third floor

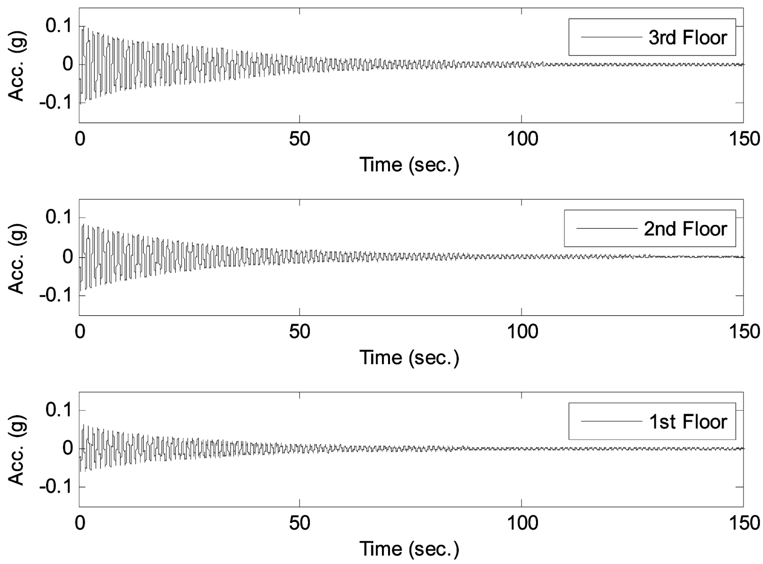

Fig. 6 Response time history of the building to free vibration

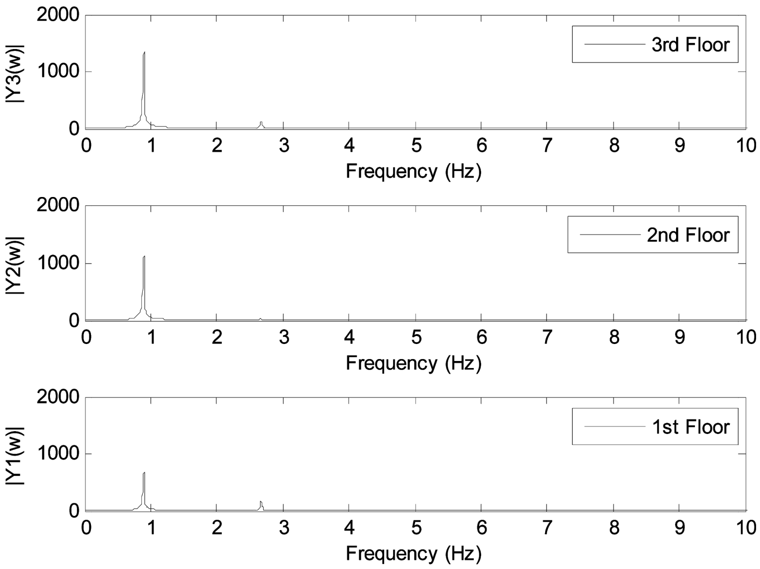

Fig. 7 Frequency responses of free vibration

frequency based on the assumption that the storey stiffness is identical. For the mass information presented earlier, the stiffness and damping matrices that give the first modal frequency of 0.90 Hz and damping ratio of 0.5% are as follows.

$$\mathbf{K}_a = \begin{bmatrix} 7348 & -3674 & 0 \\ -3674 & 7348 & -3674 \\ 0 & -3674 & 3674 \end{bmatrix} N/m \tag{8}$$

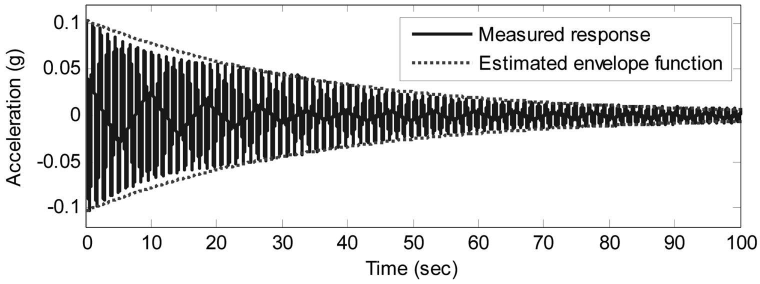

Fig. 8 Third floor response time history and estimated envelope function

$$\mathbf{C}_m = \begin{bmatrix} 13.0 & -6.5 & 0 \\ -6.5 & 13.0 & -6.5 \\ 0 & -6.5 & 6.5 \end{bmatrix} N \cdot s/m \tag{9}$$

The stiffness matrix given in Eq. (8) yields the fist mode eigenvector of $\boldsymbol{\phi}_1^T = [0.4450 \quad 0.8019 \quad 1.0]$, which differs from the measured eigenvector. In general, the eigenvector measurement exhibits more error than the natural frequency measurement. For lightly damped structure like the test building, the small change in damping affects the peak values of FRF significantly, and thereby the eigenvector is hard to be measured (Chopra 2000). The stiffness matrix in Eq. (8) and damping matrix in Eq. (9) yield the natural frequencies of 0.90 Hz, 2.52 Hz, and 3.64 Hz and modal damping ratios of 0.5%, 1.4% and 2.0%. In this study, the stiffness matrix in Eq. (8) is used as an analytically obtained stiffness matrix along with the mass matrix of $\boldsymbol{M}_a$ = diag [22.758 22.758 22.758].

3.3 White noise test

The white noise test has an advantage over the free vibration test that the information on all modes is available. FRF is obtained using measured data of 200 seconds and measured natural frequencies are 0.90 Hz, 2.68 Hz, and 3.95 Hz. The measured eigenvectors using Eq. (7) are

$$\boldsymbol{\Phi}_m = \begin{bmatrix} 0.5146 & -1.3753 & 1.1783 \\ 0.8439 & -0.3073 & -1.9783 \\ 1.0000 & 1.0000 & 1.0000 \end{bmatrix} \tag{10}$$

The stiffness matrix given in Eq. (8) is updated using Eq. (5) and measured eigenvectors given in Eq. (10). The resulting updated eigenvectors, updated stiffness matrix, and identified damping matrix are

$$\boldsymbol{\Phi}_{up} = \begin{bmatrix} 0.5338 & -1.3807 & 1.1188 \\ 0.8780 & -0.2995 & -1.8191 \\ 1.0000 & 1.0000 & 1.0000 \end{bmatrix} \tag{11}$$

$$\mathbf{K}_{up} = \begin{bmatrix} 7368 & -4083 & 40 \\ -4083 & 8822 & -4928 \\ 40 & -4928 & 5033 \end{bmatrix} N/m \tag{12}$$

$$\mathbf{C}_m = \begin{bmatrix} 5.83 & -3.46 & 1.19 \\ -3.46 & 8.56 & -3.91 \\ 1.19 & -3.91 & 5.29 \end{bmatrix} N \cdot s/m \tag{13}$$

The stiffness matrix given in Eq. (12) yields the natural frequencies of 0.9 Hz, 2.68 Hz, and 3.95 Hz, which are same to measured natural frequencies as expected. The estimated modal damping ratios are 0.83%, 0.65% and 1.2%.

3.4 State-space model using subspace method (N4SID)

Eigenvector estimation based on the peak values in measured FRF given in Eq. (7) may not give accurate results in identifying the mode shape vector for the FE model updating. For instance, frequency domain methods may yield erroneous results in cases of close modal frequencies, dissimilar peak levels, or high damping ratio especially in presence of measurement noise (Pandit 1990). In order to validate the identification results given in previous sections, the subspace algorithm using state space model is performed (Van Overschee and De Moor 1994). The algorithm estimates state sequences of dynamic systems directly from the given data, through a set of basic linear algebra operations, such as QR factorization and singular value decomposition. The extraction of the state space model is then achieved through the solution of a least squares problem. It is well known that the algorithm allows numerically reliable implementation and yields model estimations with good accuracy (Ljung 1999).

A state-space system expressing the relationship between the input vector $\boldsymbol{u}$ and the output vector $\boldsymbol{y}$ through state variable vector $\boldsymbol{z}$ can be expressed as

$$\dot{\mathbf{z}} = \mathbf{A}\mathbf{z} + \mathbf{B}\mathbf{u} \tag{14}$$

$$\mathbf{y} = \mathbf{C}\mathbf{z} + \mathbf{D}\mathbf{u} \tag{15}$$

where $\boldsymbol{A}$, $\boldsymbol{B}$, $\boldsymbol{C}$, and $\boldsymbol{D}$ are the state transition matrix, input influence matrix, output influence matrix, and direct transmission term respectively. The same white noise test data is used for the subspace algorithm, and the system matrices are obtained applying matlab function *N4SID* (Ljung 2007). The resulting system matrices are

$$\mathbf{A} = \begin{bmatrix} -0.0138 & 6.3012 & 0.0362 & 0.4475 & 0.3035 & 0.0455 \\ -5.0973 & -0.0650 & -0.0372 & -0.2475 & 0.0889 & -0.5131 \\ -0.0315 & -0.0587 & -0.0672 & -17.3059 & 0.0238 & -0.0999 \\ -0.0252 & 0.1464 & 16.4338 & -0.2021 & 0.1129 & -0.3839 \\ -0.0252 & -0.0533 & -0.1064 & 0.1994 & -0.4255 & 25.8533 \\ -0.0118 & -0.0127 & -0.0672 & 0.1260 & -23.9406 & -0.0311 \end{bmatrix} \tag{16}$$

$$\mathbf{B} = \begin{bmatrix} -2.8025 \\ -5.8781 \\ -0.3541 \\ 3.5713 \\ -0.0112 \\ -1.2222 \end{bmatrix} \tag{17}$$

$$\mathbf{C} = \begin{bmatrix} -0.4364 & 0.1835 & -1.5306 & -0.3801 & -1.2146 & 0.3088 \\ -0.7321 & 0.2880 & -0.3844 & -0.0749 & 1.9798 & -0.0598 \\ -0.8306 & 0.4657 & 1.0353 & 0.5522 & -0.9858 & 0.5642 \end{bmatrix} \tag{18}$$

$$D = \begin{bmatrix} 0 \\ 0 \\ 0 \end{bmatrix} \tag{19}$$

The complex mode shape can be extracted from identified system matrices as (Bodeux and Golinval 2001).

$$\mathbf{\Phi} = \mathbf{CL} \tag{20}$$

where $\boldsymbol{L}$ is the matrix formed with the eigenvectors of $\boldsymbol{A}$ positioned as columns. The real mode shape is then obtained by multiplying the modulus of each element of the complex mode shape vector by the sign of the cosine of its phase angle (Friswell and Mottershead 1995). The resulting measured eigenvectors are

$$\mathbf{\Phi}_m = \begin{bmatrix} 0.5137 & -1.3193 & 1.0978 \\ 0.8415 & -0.2980 & -1.7398 \\ 1.0000 & 1.0000 & 1.0000 \end{bmatrix} \tag{21}$$

It can be noticed that the measured eigenvectors using the subspace method is slightly different to ones presented in Eq. (10). The stiffness matrix given in Eq. (8) is updated using Eq. (5) and measured eigenvector given in Eq. (21) for the FE updating. The resulting updated eigenvectors, updated stiffness matrix, and identified damping matrix are

$$\mathbf{\Phi}_{up} = \begin{bmatrix} 0.5314 & -1.3689 & 1.1429 \\ 0.8809 & -0.3094 & -1.8247 \\ 1.0000 & 1.0000 & 1.0000 \end{bmatrix} \tag{22}$$

$$\mathbf{K}_{up} = \begin{bmatrix} 7450 & -4125 & 63 \\ -4125 & 8808 & -4923 \\ 63 & -4923 & 5034 \end{bmatrix} N/m \tag{23}$$

$$\mathbf{C}_m = \begin{bmatrix} 6.36 & -2.58 & -0.13 \\ -2.58 & 6.90 & -3.33 \\ -0.13 & -3.33 & 5.05 \end{bmatrix} N \cdot s/m \tag{24}$$

The stiffness matrix given in Eq. (23) yields the natural frequencies of 0.9 Hz, 2.68 Hz, and 3.96 Hz, which are closed to ones estimated in previous section. The estimated modal damping ratios are 0.68%, 0.75% and 0.87%.

3.5 Comparison of methods

In order to evaluate the identified and the updated model parameters, the modal assurance criterion (MAC) values between the experimental and FE mode shapes are calculated. The MAC value is often used to compare the relative similarity between two mode shapes (Friswell and Mottershead 1995). The MAC is generally defined as

$$MAC(\phi_i, \phi_j) = \frac{(\phi_i^T \phi_j)^2}{(\phi_i^T \phi_i)(\phi_j^T \phi_j)} \tag{25}$$

In Table 2, the results of MAC values between the experimental and FE mode shapes are summarized. The experimental mode shapes are ones presented in Eq. (21), which is obtained using the subspace algorithm. The initial FE model indicates the system with stiffness matrix presented in Eq. (8), which is obtained from the free vibration test. The updated FE models are the systems with updated stiffness matrices presented in Eqs. (12) and (23), which are both obtained from the white noise test but using different identification methods. It is observed from Table 2 that the updated mode shapes yields MAC values closer to one than the initial FE model indicating that the FE

Table 2 MAC values between the experimental and FE models

	1st mode	2nd mode	3rd mode
Initial FE model	0.9984	0.9751	0.9753
Updated FE model (Eq. 11)	0.9995	0.9997	0.9997
Updated FE model (Eq. 22)	0.9995	0.9997	0.9997

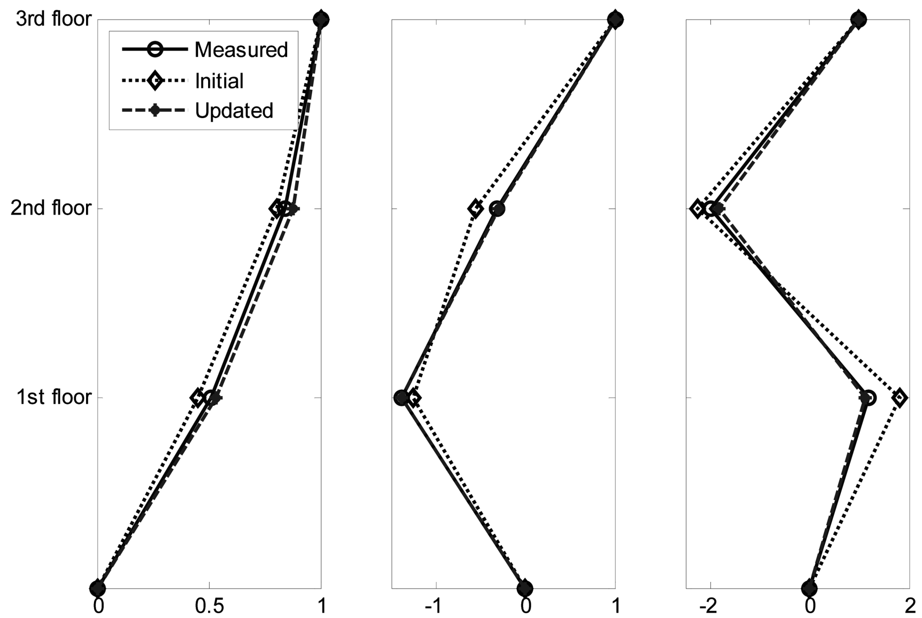

(a) 1st mode (b) 2nd mode (c) 3rd mode

Fig. 9 Mode shape comparison

updating based on the white noise test data results in closer mode shapes to measured ones. The same observation also can be noticed in Fig. 9 where the updated mode shapes are compared to the experimental ones. It is shown that the updated stiffness matrix yields mode shapes closer to measured ones compared to initial model shape. In Fig. 9, the experimental and updated mode shapes from the subspace algorithm are only presented because eigenvectors estimated based on the peak values in measured FRF yields very similar results as shown in Table 2.

The comparison of the FRFs for absolute acceleration of the each floor from ground acceleration is presented in Figs. 10 to 12. The estimated FRFs obtained using free vibration responses matches only in the first mode and peaks of the second and third mode differ from those of experiment. This is because only information on the first mode is identified and the second and third modes are obtained from the stiffness matrix that is constructed assuming identical storey stiffness. The estimated FRF obtained using white noise responses and the FE updating matches well to experimental result for all three modes. It is noted that the FRF estimated using the updated stiffness matrix by the subspace algorithm (indicated as *N4SID*) is very close to one estimated using the

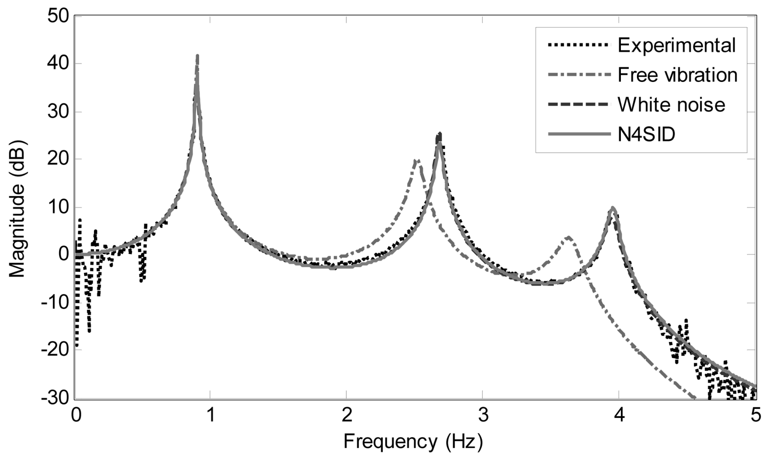

Fig. 10 Comparison of the FRF for absolute acceleration of the third floor from ground acceleration

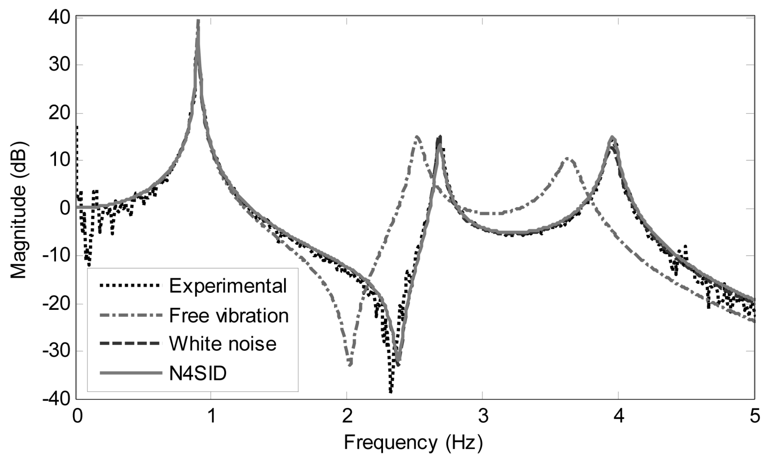

Fig. 11 Comparison of the FRF for absolute acceleration of the second floor from ground acceleration

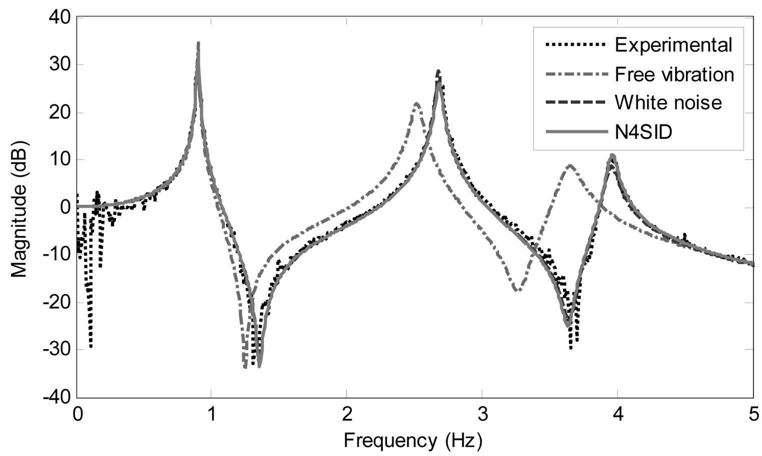

Fig. 12 Comparison of the FRF for absolute acceleration of the first floor from ground acceleration

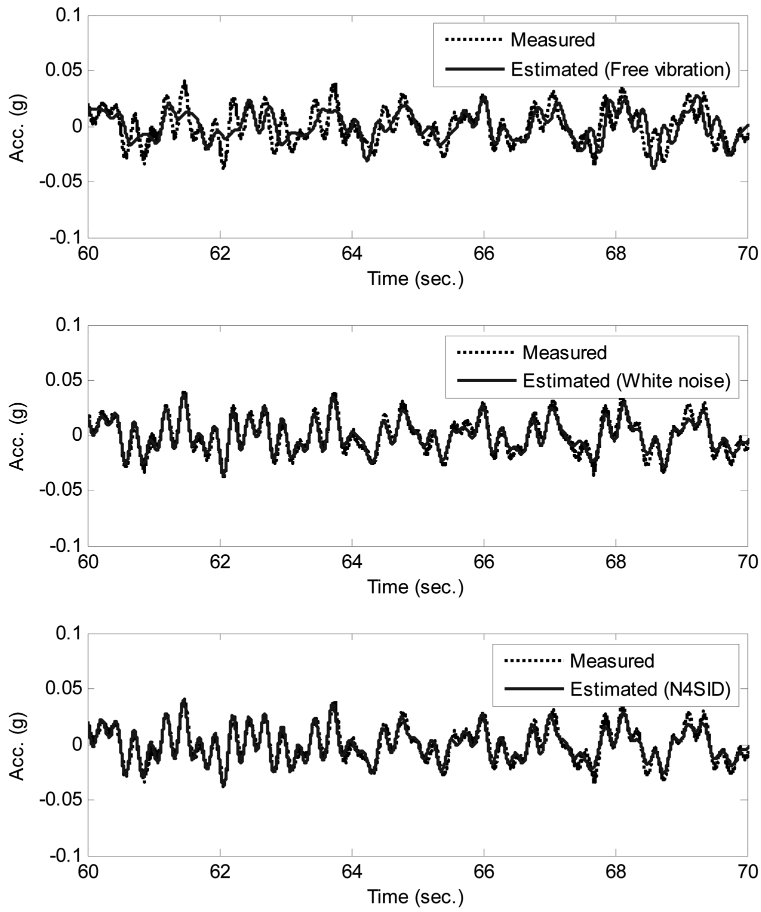

Fig. 13 Acceleration time history of second floor subjected to white noise ground motion

updated stiffness matrix based on the peak values in measured FRF (indicated as *White noise*).

In Fig. 13, the acceleration time histories of second floor subjected to white noise ground motion are presented. As in the comparison of FRF, the estimated time histories using updated stiffness matrices match well to the measured ones, while the estimated time histories using the stiffness matrix obtained from free vibration responses show limited similarity.

4. System Identification of a building using PZT

For the system identification using PZT, the building responses are measured with PZT patches. PZT patches are used as sensors only and the building is vibrated using the same shaking table. Five PZT patches are attached on each storey column and free vibration and white noise test are performed (Fig. 14). The PZT patch used for testing is a disk type patch, produced by East-Mingtao Electronics. The diameter of PZT patch is 20 mm and thickness is 0.4 mm. This PZT patch is selected due to its very low cost which is less than one US Dollar. The output voltage of PZT patch is measured using NI PXU-1042Q.

The frequency responses obtained using responses to white noise input are presented in Fig. 15. It is shown that the natural frequencies of three modes are identifiable from the white noise test. Since the structure is vibrated by shaking table, not by PZT itself, the impedance function is not obtained. Instead, the measured natural frequencies are used for FE updating for the system identification.

The updated stiffness matrix is obtained using Eq. (5) updating the stiffness matrix given in Eq. (8), which is analytically obtained assuming same storey stiffness of 3.674 kN/m. Since the eigenvector is not available, the analytically obtained eigenvector is used for the stiffness updating. The measured natural frequencies are 0.90 Hz, 2.68 Hz, and 3.95 Hz, and the resulting updated stiffness matrix is

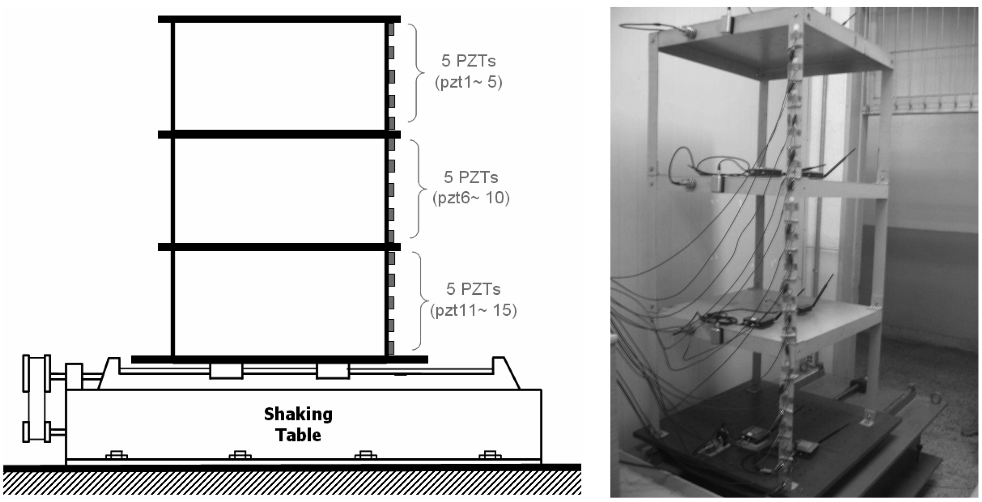

(a) Schematic of shaking table experiment (b) Experimental setup

Fig. 14 Shaking table experiment of a three storey building with PZT sensors

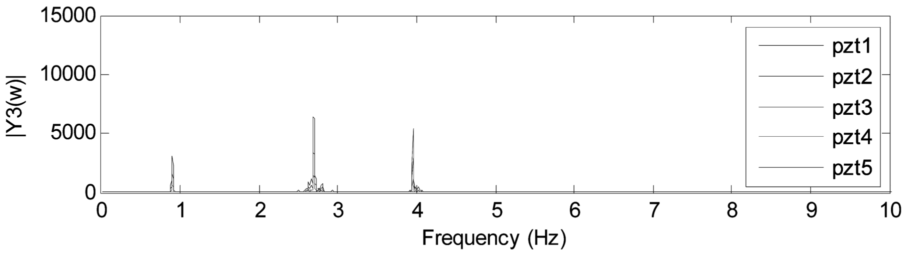

(a) Frequency responses of PZTs on the third floor column

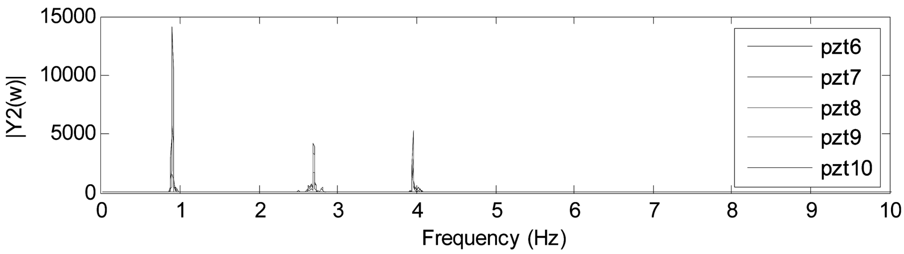

(b) Frequency responses of PZTs on the second floor column

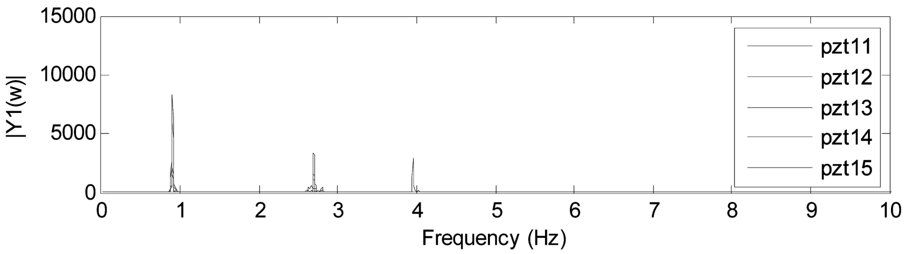

(c) Frequency responses of PZTs on the first floor column

Fig. 15 Frequency responses of PZTs on columns – white noise test

$$\mathbf{K}_{up} = \begin{bmatrix} 8488 & -4415 & 87 \\ -4415 & 8575 & -4328 \\ 87 & -4328 & 4160 \end{bmatrix} kN/m \tag{26}$$

In Fig. 16, The FRF for absolute acceleration of the second floor from ground acceleration obtained using PZT patches is compared with those obtained experimentally and estimated using MEMS in previous section. In Fig. 17, the acceleration time histories of second floor subjected to white noise ground motion are presented. It can be seen from Fig. 16 that the peaks identified using PZT sensors match well to those obtained experimentally since all natural frequencies are measured. This indicates that even though limited information is available, PZT sensing yields reliable system identification results. Considering very low cost and ease of installation, the PZT sensor in the system identification of building structures is an effective material.

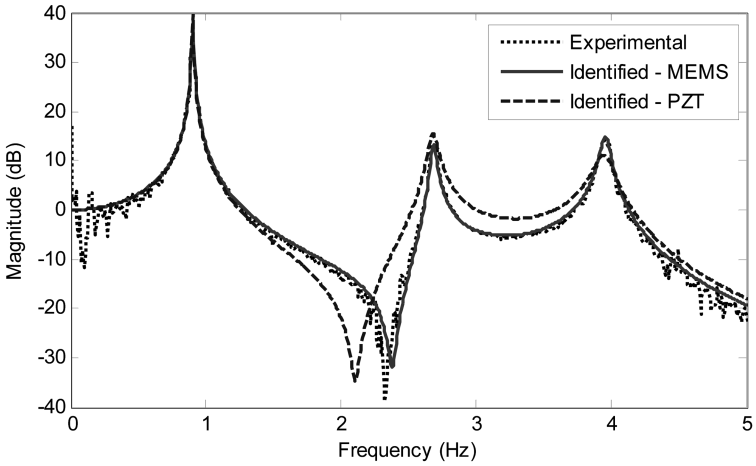

Fig. 16 Comparison of the FRF for absolute acceleration of the second floor from ground acceleration

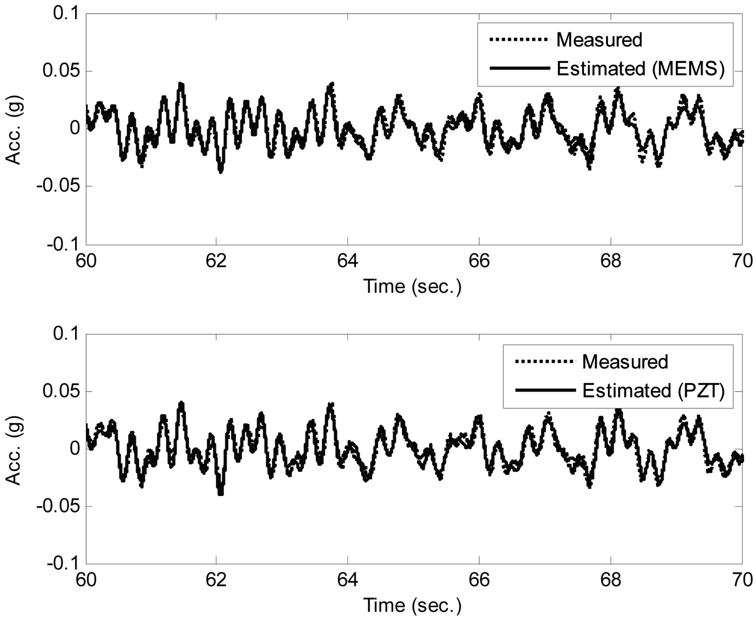

Fig. 17 Acceleration time history of second floor subjected to white noise ground motion

5. Conclusions

The structural monitoring system based on cheap and wireless monitoring system is investigated using MEMS based accelerometer. The system identification using wireless MEMS is evaluated experimentally using a three storey frame model and identification results are compared to ones using the data measured using traditional accelerometers. The FE model updating is used for the system identification using wireless MEMS. A free vibration test and white noise test are performed to validate the system identification using wireless MEMS accelerometers. The estimated FRF obtained using free vibration responses matches only in the first mode and peaks of the second and third mode differ from those of experiment. This is because only information on the first mode is identified and the second and third modes are obtained from the stiffness matrix that is constructed assuming identical storey stiffness. In practice, it is not easy to perform a free vibration test in a real building structure without the aid of exciting machine. Therefore, the free vibration test has limited applicability in structural health monitoring. On the other hand, the estimated FRF obtained using white noise responses and the FE updating matches well to the experimental result for all three modes. It is also found that the updated mode shapes yields MAC values closer to one than the initial FE model indicating that the FE updating based on the white noise test data results in closer mode shapes to measured ones.

Another smart sensor considered in this paper for structural health monitoring is the PZT patch. The system identification for building structures by using PZT patched that function as sensor only is presented. The FE model updating method is applied with the experimental data obtained using PZT patches, and results are compared to ones obtained using wireless MEMS system. Using PZT patches, it is only possible to obtain natural frequencies by measuring strain response of columns of which PZT is bonded, while mode shape vectors of structures are not obtainable. Consequently, the only peaks in FRF identified using PZT sensors match to those obtained experimentally. Considering very low cost and ease of installation, the PZT sensor in the system identification of building structures can be effective if the natural frequencies are of concern.

Acknowledgements

This work was supported by the Korea Science and Engineering Foundation (KOSEF) grant funded by the Korea government (MOST) (No.R11-2002-101-01002-0(2007)) and by the Korea Research Foundation Grant funded by the Korean Government (MOEHRD) (The Regional Research Universities Program/Biohousing Research Institute).

References

Analog Devices, *ADXL103 Data Sheets*, http://analog.com

Baruch, M. (1978), “Optimization procedure to correct stiffness and flexibility matrices using vibration tests”, *AIAA J.,* **16**(11), 1208-1210.

Baruch, M. and Bar-Itzhack, I.Y. (1978), “Optimal weighted orthogonalization of measured modes”, *AIAA J.*, **16**(11), 346-351.

Bhalla, S. and Soh, C.K. (2004), “High frequency piezoelectric signatures for diagnosis of seismic/blast induced structural damages”, *NDT & E Int.*, **37**(1), 23-33.

Chopra, A.K. (2000), *Dynamics of Structures: Theory and Applications to Earthquake Engineering*, Prentice Hall, NJ.

East Mingtao, Piezo *Element with Lead Wire*, http://east-mingtao.com

Friswell, M.I. and Mottershead, J.E. (1995), *Finite Element Model Updating in Structural Dynamics*, Kluwer Academic Publishers, Netherlands.

Gao, Y. and Spencer, Jr. B.F. (2007), “Experimental verification of a distributed computing strategy for structural health monitoring”, *Smart Struct. Syst*., **3**(4), 455-474.

Helvajian, H. (1999), *Microengineering Aerospace Systems*, Aerospace Press Series, AIAA.

Hierold, C. (2004), “From micro- to nanosystems: Mechanical sensors go nano”, *J. Micromech. Microeng.,* **14**,

S1-S11.
Kinawi, H., Taha, M.M.R. and El-Sheimy N. (2002), "Structural health monitoring using the semantic wireless: A novel application for wireless networking", *Proceedings of the 27th Annual IEEE Conference on Local Computer Networks*, Tampa, Florida, November.

Krüger, M., Große, C.U. and Marrón, P.J. (2005), "Wireless structural health monitoring using MEMS", *Key Eng. Mater.*, **293-295**, 625-634.

Lance Measurement Technologies, *Built-in IC Piezoelectric Accelerometers,* http://www.lancetec.com

Lee, J.J. and Yun, C.B. (2006), "Two-step approaches for effective bridge health monitoring", *Struct. Eng. Mech*., **23**(1), 75-95.

Li, C. and Reinhorn, J.C. (1995), "Experimental and analytical investigation of seismic retrofit of structures with supplemental damping: Part II – friction devices", *Technical Report NCEER-95-0009*, National Centre for Earthquake Engineering Research, Buffalo, NY.

Lin, R.M. and Wang, W.J. (2006), "Structural dynamics of Microsystems - current state of research and future directions", *Mech. Sys. Signal Pr.*, **20**, 1015-1043.

Lynch, J.P., Partridge, A., Law, K.H., Kenny, T.W., Kiremidjian, A.S. and Carryer, E. (2003), "Design of piezoresistive MEMS-based accelerometer for integration with wireless sensing unit for structural monitoring", *J. Aerospace Eng.*, **16**(3), 108-114.

Ljung, L. (2007), *System Identification Toolbox User's Guide*, Mathworks.

Obadat, M., Lee, H., Bhatti, M.A. and Maclean, B. (2003), "Full-scale field evaluation of microelectromechanical system-based biaxial strain transducer and its application in fatigue analysis", *J. Aerospace Eng.*, **16**(3), 100-107.

Park, G., Sohn, H., Farrar, C.R. and Inman, D.J. (2003), "Overview of piezoelectric impedance-based health monitoring and path forward", *Shock Vib.*, **35**(6), 451-463.

Pandit, S.M. (1991), *Modal and Spectrum Analysis: Data Dependent Systems in State Space*, Wiley Interscience, New York.

Shinozuka, M., Feng, M.Q., Chou, P., Chen, Y. and Park, C. (2003), "MEMS-based wireless real-time health monitoring of bridges", *Proceedings of the 3rd International Conference on Earthquake Engineering,* Nanjing, China, October.

Soh, C.K., Tseng, K.K-H., Bhalla, S. and Gupta, A. (2000), "Performance of smart piezoceramic patches in health monitoring of a RC bridge", *Smart Mater. Struct.*, **9**(4), 533-543.

Staszewski, W., Boller, C. and Tomlinson, G.R. (2004), *Health Monitoring of Aerospace Structures: Smart Sensor Technologies and Signal Processing*, John Wiley and Sons, England.

Tseng, K.K. and Wang, L. (2004), "Smart piezoelectric transducers for in situ health monitoring of concrete", *Smart Mater. Struct.*, **13**, 1017-1024.

Van Overschee, P. and Demoor , B. (1994), "N4SID: Subspace algorithms for the Identification of Combined Deterministic-Stochastic Systems", *Automatica*, **30**(1), 75-93.

Vittorio, S.A. (2001), "MicroElectroMechanical Systems (MEMS)," *Cambridge Scientific Abstracts*, October, 1-11.

Zhang, Y., Cheng, L. and Naito, C. (2005), "A study of wireless MEMS accelerometers for civil infrastructure monitoring", *Technical Report LU-CSE-05-015*, Department of Computer Science and Engineering, Lehigh University.